Marine Pollution Bulletin 58 (2009) 238–248

Contents lists available at ScienceDirect

Marine Pollution Bulletin

journal homepage: www.elsevier.com/locate/marpolbul

Application of HF radar currents to oil spill modelling

Ana J. Abascal [a,*], Sonia Castanedo [a], Raul Medina [a], Inigo J. Losada [a], Enrique Alvarez-Fanjul [b]

[a] Environmental Hydraulics Institute (IH Cantabria), Universidad de Cantabria, Avda. de los Castros s/n. 39005, Santander, Spain
[b] Área de Medio Físico. Puertos del Estado (PdE), Madrid, Spain

ARTICLE INFO

Keywords:
HF radar currents
Lagrangian transport model
Drifter buoy
Oil spill trajectory

ABSTRACT

In this work, the benefits of high-frequency (HF) radar currents for oil spill modeling and trajectory analysis of floating objects are analyzed. The HF radar performance is evaluated by means of comparison between a drifter buoy trajectory and the one simulated using a Lagrangian trajectory model. A methodology to optimize the transport model performance and to calculate the search area of the predicted positions is proposed. This method is applied to data collected during the Galicia HF Radar Experience. This experiment was carried out to explore the capabilities of this technology for operational monitoring along the Spanish coast. Two long-range HF radar stations were installed and operated between November 2005 and February 2006 on the Galician coast. In addition, a drifter buoy was released inside the coverage area of the radar. The HF radar currents, as well as numerical wind data were used to simulate the buoy trajectory using the TESEO oil spill transport model. In order to evaluate the contribution of HF radar currents to trajectory analysis, two simulation alternatives were carried out. In the first one, wind data were used to simulate the motion of the buoy. In the second alternative, surface currents from the HF radar were also taken into account. For each alternative, the model was calibrated by means of the global optimization algorithm SCEM-UA (Shuffled Complex Evolution Metropolis) in order to obtain the probability density function of the model parameters. The buoy trajectory was computed for 24 h intervals using a Monte Carlo approach based on the results provided in the calibration process. A bivariate kernel estimator was applied to determine the 95% confidence areas. The analysis performed showed that simulated trajectories integrating HF radar currents are more accurate than those obtained considering only wind numerical data. After a 24 h period, the error in the final simulated position improves using HF radar currents. Averaging the information from all the simulated daily periods, the mean search and rescue area calculated using HF radar currents, is reduced by approximately a 62% in comparison with the search area calculated without these data. These results show the positive contribution of HF radar currents for trajectory analysis, and demonstrate that these data combined with atmospheric forecast models, are of value for trajectory analysis of oil spills or floating objects.

1. Introduction

The number of accidental oil spills on the Spanish coast has led to a growing concern regarding oil spill response, and has motivated the development and implementation of operational tools to be used in these emergency situations (Alvarez-Fanjul et al., 2007). A summary of the oil spills around the Spanish coast in the last decades is shown in Fig. 1. Most of the accidents are located along the Galician coast and the Strait of Gibraltar. Although both areas have intense maritime traffic and are vulnerable to potential spills, it is observed that the most important accidents are located on the Galician coast. The following accidents are worth mentioning due to their importance: *Urquiola* 1976, *Andros Patria* 1978, *Aegean Sea* 1992 and most recently the *Prestige* in 2002. This last accident caused one of the largest oil pollution related catastrophes on the Spanish coast. The *Prestige,* carrying approximately 77,000 tons of heavy oil, began to leak approximately 30 nautical miles off the Galician coast on November 13th, 2002. The ship split in half and sank on November 19th spilling about 63,000 tons (Castanedo et al., 2006) and affecting more than 2000 km of shoreline (Ministerio de Medio Ambiente, 2005). The experience acquired in the management of the *Prestige* crisis demonstrated the importance of operational forecasting systems in the oil spill response (Montero et al., 2003; Castanedo et al., 2006; González et al., 2006).

In an oil spill emergency, the main functions of an operational system are to forecast ocean and weather conditions as well as oil spill trajectories to provide decision makers with a technical assessment to respond to the crisis. The application of oil spill numerical models to forecast oil slick trajectories is an essential

* Corresponding author. Tel.: +34 942 201810; fax: +34 942 201860.
E-mail address: abascalaj@unican.es (A.J. Abascal).

0025-326X/$ - see front matter © 2008 Elsevier Ltd. All rights reserved.
doi:10.1016/j.marpolbul.2008.09.020

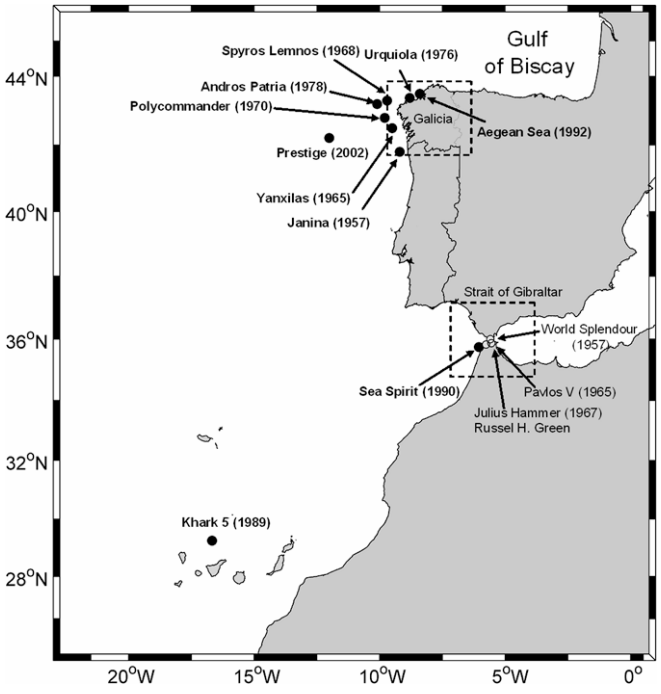

Fig. 1. Summary of accidental spills having affected the coast of Spain in the last decades (adapted from www.cedre.fr). Spillages greater than 10000 tonnes are represented by black circles and bold names; spillages lower than 10000 tonnes by grey circles. location of Galicia region and the Strait of Gibraltar is presented (dashed-boxes).

component of an operational system. The success of its application depends on the formulation of the model itself, and also on the accuracy of the input data (wind, waves and currents), usually provided by numerical models (Sebastiao and Soares, 2006). These atmospheric and oceanographic models have their own errors which may affect the accuracy of the oil spill forecasts (Edwards et al., 2006; Price et al., 2006). The uncertainty becomes more important in the ocean circulation modeling of coastal areas, where the complex pattern that characterizes the slope currents complicates the forecasting of the current field. Abascal et al. (2009) using drifting buoys deployed during the *Prestige* accident, showed that the bigger differences between simulated and actual trajectories were found in buoys deployed over the continental slope. Although two state-of-the-art global ocean circulation models were used in this study, the results showed that further work is needed in modeling ocean currents in order to have reliable simulated data in coastal areas. Some of these advances, such as employing higher resolution nested models, are already being developed. For example, Sotillo et al. (2008) obtained an evident improvement in the buoys trajectories forecast in the continental shelf of the Gulf of Biscay when including the currents generated by ESEOAT, a 3D high resolution nested model, as forcing field. However, even this new generation models are not accurate and reliable enough to provide a satisfactory reply at any time and domain.

Therefore, the forecasting of the current field is the least reliable and most undeveloped part of the operational systems. As a consequence, the traditional operational response method to oil spills does not take into account the currents as a forcing of the trajectory models. This approach is particularly well suited to areas where the wind drift is the main forcing of the floating pollutant. However, there are certain areas in which the transport induced by ocean currents could not be ignored in the simulation of the oil spill motion. Abascal et al. (2009) showed that while buoys trajectories located outward the continental slope of the Gulf of Biscay were dominated by the wind forces, a joint wind and currents effect was required to reproduce the buoys trajectories in the shelf slope and coastal areas. Caballero et al. (2008) used a semi-empirical ocean model to simulate the trajectory of a drifter buoy deployed during the *Prestige* accident, and they found that the model reproduced relatively well the trajectory followed by the drifter.

All these studies show that high quality currents data are required in order to provide reliable results in an oil spill response. In recent years important efforts have been carried out to develop the operational oceanography (Nittis et al., 2001; Pinardi et al., 2003; Sotillo et al., 2008) and data from circulation models has becoming available. However, the accuracy of the solutions is limited due to the scarce real time ocean data available for assimilation. To address this problem, high frequency radar systems become an alternative to provide accuracy surface current maps in near coastal environments. The radar systems are capable of spatially measuring dense surface currents in real time and could be used as input for oil spill trajectory models in an emergency response at sea. HF radar surface currents have been validated with many different types of *in situ* current measurements, including surface drifters and subsurface current meters (Kohut et al., 2006). The accuracy of these measurements has been reported to be between 9 and 27 cm/s. A general review of the validation studies can be found in Chapman et al. (1997) and Chapman and Graber (1997). These works show that the remote sensing of surface currents in coastal areas using HF radar systems is an accurate technology (Chapman et al., 1997), being suitable for many oceanographic applications, such as oil spill response and maritime search and rescue (Hodgins, 1991). Due to the new capabilities offered by this technology, several studies have been taken place to assess the effectiveness of trajectory analysis using currents derived from HF radar (Ullman et al., 2003, 2006; O'Donnell et al., 2005).

To explore the capabilities of HF radar for operational monitoring on the Spanish coast, the Galicia HF Radar Experience has been carried out by the Spanish institution Puertos del Estado, Qualitas Instruments and the Port Authorities of Vigo and La Coruña. During the experiment, two long-range HF radar stations were installed and operated from November 2005 to February 2006 in the Galician coast, the main area affected by the *Prestige* disaster. In addition, a drifter buoy was released inside the coverage area of the radar.

The main objective of this paper is to investigate the benefits of using HF radar currents for oil spill modelling and trajectory forecast of floating objects. The HF radar performance is evaluated by means of comparison between the actual drifter buoy trajectory and the one simulated using a Lagrangian trajectory model. A methodology is developed and applied to optimize the transport model performance and to calculate the search area of the predicted positions. Two alternatives of simulation are carried out: (1) the first experiment is performed using wind numerical data to simulate the buoy trajectory assuming negligible currents with respect to the wind forcing, (2) in the second experiment, observed HF radar currents are additionally considered to reproduce the motion of the buoy. Firstly, the transport model is calibrated by means of a global optimization algorithm in order to obtain the optimal model parameters and their corresponding 95% confidence interval for each proposed alternative. Subsequently, the calibration results are used to compute the buoy trajectory using a Monte Carlo approach. Finally, the 95% confidence areas are determined by means of a bivariate kernel estimator. The Galicia HF Radar Experience and the feasibility study performed, represent the first attempt to analyze the benefit of using HF radar technology for operational monitoring and oil spill response on the Spanish coast.

2. Data and methodology

2.1. Experiment description

The Galicia HF Radar Experience was established to study the advantages of integrating the emerging HF radar technology into existing Puertos del Estado monitoring systems. From an administrative point of view, it was developed as a collaboration agreement between Puertos del Estado, the private company Qualitas–Remos and the Port Authorities of A Coruña and Vigo. Two long range SeaSonde CODAR (Coastal Ocean Dynamics Applications Radar) HF radars were installed in the lighthouses of Silleiro and Fisterra (see Fig. 2) and operated during a period of three months. The new instruments became part of the operational networks of Puertos del Estado. During this period all the data produced were freely distributed in real time through the Puertos del Estado web page.

The experience was designed in such a way that the Silleiro Station, one of the Puertos del Estado Deep Water Network buoys (Alvarez-Fanjul et al., 2003), was located in the area covered by the radar (Fig. 2). The deep water buoy, equipped with a UCM-60 sensor for current measurements at a depth of 3 m, was used to analyze the reliability of the currents data obtained by the radar systems (Alfonso et al., 2006).

In addition, a PTR surface drifting-buoy (see Fig. 3) was released inside the radar coverage area with the purpose of providing data to analyze the feasibility of using the HF radar technology for trajectory forecast purposes. The buoy was tracked by the ARGOS satellite-based system and remained inside the coverage area from December 2005 to January 2006.

2.2. Data

The radar systems were deployed from November 2005 to February 2006. The CODAR radars were operated at 4.5 MHz and provided hourly surface currents at 6 km resolution over the region shown in Fig. 2. In a previous study, these data were compared with in situ current measurements provided by the deep buoy of Puertos del Estado (see Fig. 2) (Alfonso et al., 2006). These authors found a good agreement between HF radar and the moored buoy. The root mean square error calculated in this study was in the range of variation reported in the literature (Chapman et al., 1997; Chapman and Graber, 1997; Kohut et al., 2006).

Although the coverage area of the radar ranges up to 180 km, the extent of the area within which long range CODAR data are available varies. Due to the drop in height of the ionosphere, the range is significantly reduced during the night. As an example of this variability, a night-time and a daytime current map, produced by CODAR during the experiment, are shown in Fig. 2a and b, respectively.

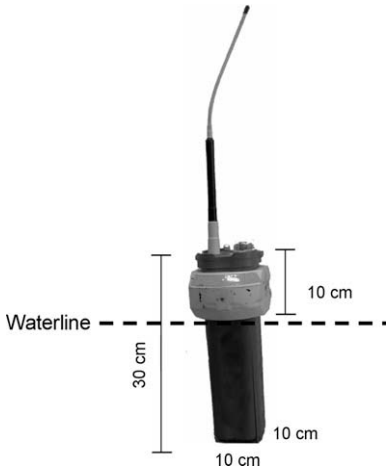

Fig. 3. PTR surface drifting-buoy. The dimensions of the buoy and the waterline (dashed-line) are shown.

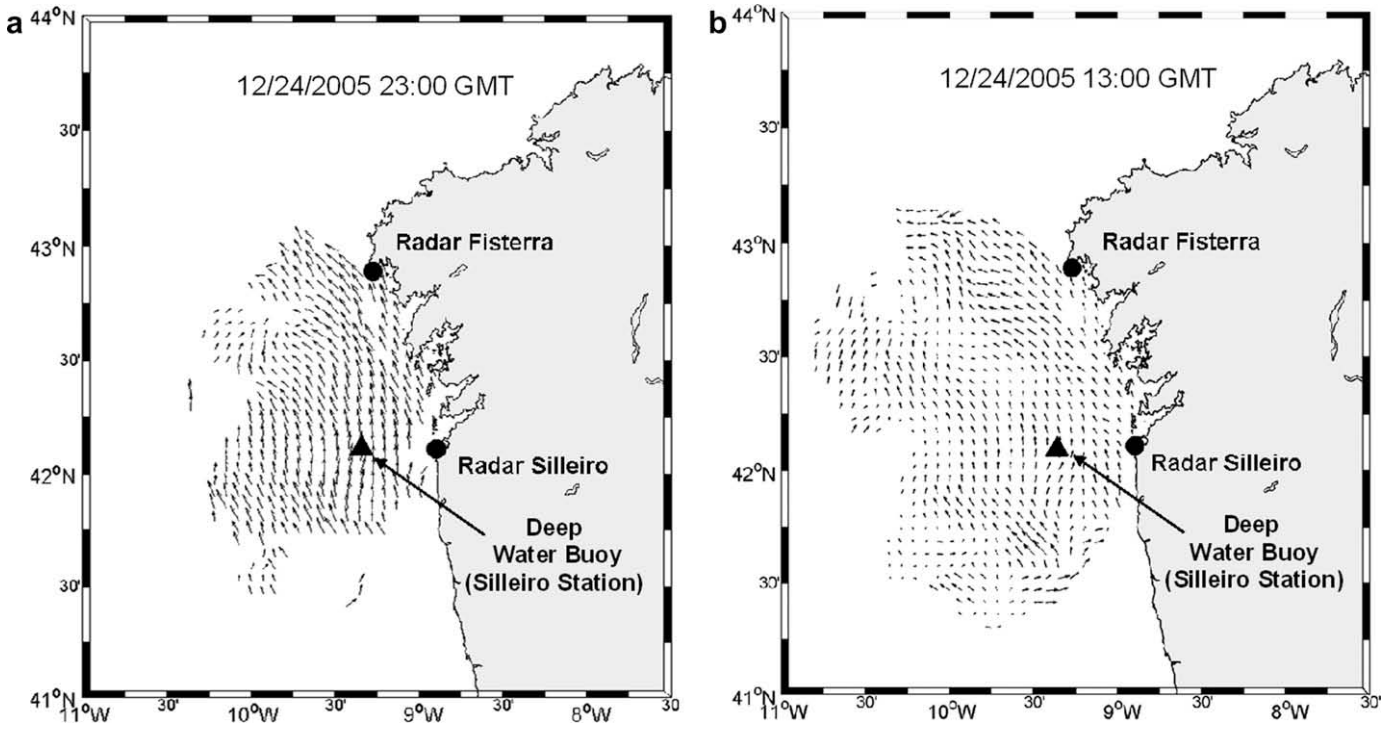

Fig. 2. Typical surface current map produced by CODAR showing the coverage area of the radar: (a) night-time surface current map on 12/24/2005 23:00 GMT and (b) daily surface current map on 12/24/2005 13:00 GMT. The radar site locations (Silleiro and Fisterra) are indicated by solid black circles. The deep water buoy is also shown (triangle).

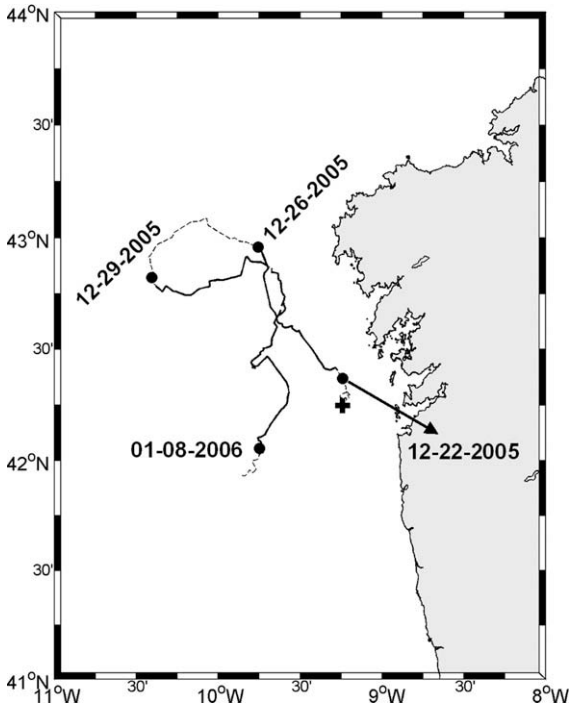

Fig. 4. Trajectory of the surface drifter deployed during the Galicia HF Radar Experience. The black cross shows the release point of the drifter. The black circles and dates indicate the periods during which the buoy is completely inside the coverage area of the radar. Buoy positions outside this area are represented by the dashed line.

The drifter buoy was deployed on December 19th 2005 close to the Silleiro radar station. Fig. 4 shows the path followed by the buoy during the study period, which spans from December 19th 2005 to January 9th 2006. As can be seen, the drifter moved towards the North during the first days after the deployment. From the 26th of December it reversed the direction and started to move first towards the West and later in an Eastern direction, drifting finally to the South along the Galician coast. Due to the buoy track and the variability of the radar coverage area (see Fig. 2), the buoy left and then returned to the radar domain on several occasions. It remained inside the coverage area of the radar for two long periods, from the 22nd to the 26th of December 2005 and from the 29th of December 2005 to the 8th of January 2006. These are the periods considered for analysis in this work (see Fig. 4).

The atmospheric and wave 2D forcing fields were obtained from the operational systems of the Spanish Meteorological Agency (AEMET) and Puertos del Estado (Carretero et al., 2000), respectively. In both cases, only model analysis, more accurate than forecast fields, were employed. The wind fields were generated by the HIRLAM (High Resolution Limited Area Model) model (Cats and Wolters, 1996). The data consists in 10 m wind speed and direction, provided with a 0.05° spatial resolution and with a 6 h time interval. Sea state conditions were the output of the numerical model WAM, a third generation spectral wave generation model (Komen et al., 1994; WAMDIG (The Wave Model Development and Implementation Group, 1988). The WAM model solves the energy transfer equation for the wave spectrum. The model grid resolution was 0.25° and the results were the significant wave height, mean direction and mean period for sea and swell components with a 3 h time interval.

2.3. Methodology

To study the benefits of using the HF current fields for trajectory analysis, comparisons between actual and simulated trajectories of a drifter buoy were performed by means of a Lagrangian trajectory model. Two alternatives of simulation were carried out with the objective of evaluating the contribution of HF radar currents relative to the normally used environmental data sources. The first alternative (alternative 1) was performed considering that the current effect could be ignored compared to the effect of the wind. This assumption is commonly accepted in operational oil spill modelling. In the second alternative (alternative 2) in addition to atmospheric data, measured HF radar currents were taken into account to analyze the buoy motion. For each proposed alternative the Lagrangian transport model was calibrated to minimize the global difference regarding the actual buoy trajectory during the whole available data period. As a result of the calibration process, the optimum mean value and the corresponding 95% confidence interval for each model parameter was obtained. Once calibrated, the model was used to perform the final simulations, consisting of daily trajectory analysis. This procedure has two advantages: (a) the model tuning is realistic in the sense that it is obtained with the larger available data set and therefore is not specific for any given day and (b) by re-starting the simulation on a daily basis, the accumulated position error is eliminated, allowing the use of appropriate data for the trajectory simulations. Each 24 h period was computed by means of a Monte Carlo approach using the results obtained in the calibration process. The 95% confidence areas were determined and used to calculate the distance between the actual and numerical trajectories. The accuracy of the analysis was quantified by means of key statistical parameters, such as correlation factors and root mean square errors.

In this section, the Lagrangian transport model and the calibration methodology are described.

2.3.1. Lagrangian transport model

The model used in this work is the operational oil spill model called TESEO (Abascal et al., 2007). The numerical model consists of a transport and a weathering module to represent the evolution of oil spilled in the marine environment. This work focuses on the use of the transport module to analyze the motion of the surface drifter deployed in the Galicia Experience. The transport application derives from the two-dimensional Lagrangian transport model PICHI, developed by the University of Cantabria as part of the operational forecasting system created in response to the *Prestige* oil spill (Castanedo et al., 2006). The drift process of the spilled oil is described by tracking a cloud of numerical particles equivalent to the oil slicks. The position of the particles is computed by the superposition of the transport induced by currents, wind, waves and turbulent dispersion. The numerical model solves the following vector equation:

$$\frac{d\vec{x}}{dt} = \vec{u}_a(\vec{x}_i, t) + \vec{u}_d(\vec{x}_i, t) \quad (1)$$

where $\vec{x}_i$ is the particle position, and $\vec{u}_a$ and $\vec{u}_d$ are the advective and diffusive velocities respectively in $\vec{x}_i$. The advective velocity, $\vec{u}_a$, is calculated as the linear combination of currents and wind velocity and wave-induced Stokes drift, expressed as

$$\vec{u}_a = C_C\vec{u}_c + C_D\vec{u}_w + C_H\vec{u}_H \quad (2)$$

where $\vec{u}_c$ is the surface current velocity; $\vec{u}_w$ is the wind velocity at a height of 10 m over the sea surface; $\vec{u}_H$ is the wave-induced Stokes drift, calculated as $u_H = (gH/8c)$, where g is the gravitational acceleration; H is the wave height and c is the wave celerity (Dean and Dalrymple, 1991). C_D is the wind drag coefficient and C_H is the wave coefficient.

Note that Eq. (2) includes a coefficient in the currents term, C_C. Usually in Lagrangian models, the current term is not affected by any coefficient. However, to take into account the uncertainty in the radar measurements and in the numerical modeling, it was

decided to include this coefficient to minimize the differences between actual and numerical trajectories.

The turbulent diffusive velocity is obtained using a Monte Carlo sampling in the range of velocities $[-\vec{u}_d, \vec{u}_d]$ that are assumed proportional to the diffusion coefficients (Maier-Reimer, 1982; Hunter et al., 1993). The velocity fluctuation for each time step Δt, is defined as:

$$|\vec{u}_d| = \sqrt{\frac{6D}{\Delta t}} \tag{3}$$

where D is the diffusion coefficient.

2.3.2. Transport model calibration

To apply Eq. (1) the model coefficients, C_H, C_D, and C_C, have to be determined. The value of the wind drag coefficient, C_D, varies from 2.5% to 4.4% of the wind speed, with a mean value of 3–3.5% (ASCE, 1996). Reed et al. (1994) suggests that, in light winds without breaking waves, 3.5% of the wind speed in the direction of the wind gives a good simulation of oil slick drift in offshore areas. Castanedo et al. (2006) simulated buoy trajectories during the *Prestige* accident and found that a C_H around 0.05–1.5% of the wave-induced Stokes drift provided the best fit between the actual and numerical trajectories. Although it is possible to use coefficients that range between those reported in the literature, the work presented in Abascal et al. (2009) shows the importance of obtaining the best agreement model coefficients for the region of interest.

Therefore, the model calibration aims to find the optimal values of the model coefficients so as to minimize the global differences between numerical and actual trajectories provided by drifter observations.

In this study, the optimal coefficients of the model were obtained by means of the global optimization algorithm Shuffled Complex Evolution Metropolis (SCEM-UA) developed by the University of Arizona and the University of Amsterdam (Vrugt et al., 2003a,b). The SCEM-UA method is a general-purpose global optimization algorithm designed to infer the probability density function of the model parameters within a single optimization run (Vrugt et al., 2003a,b). This algorithm is a modified version of the original SCE-UA global optimization algorithm developed by Duan et al. (1992). The goal of the original SCE-UA algorithm is to find a single best parameter set in the feasible space. However, the SCEM-UA is able to infer both the most likely parameter set and its underlying posterior probability distribution. The SCEM-UA algorithm operates by merging the strengths of the Metropolis algorithm, controlled random search, competitive evolution, and complex shuffling in order to continuously update the proposal distribution and evolve the sampler to the posterior target distribution (Vrugt et al., 2003a,b).

Following this methodology, the calibration of the transport model was formulated as an optimization problem, where an objective function, J, has to be minimized. In this case, the objective function was defined as

$$J(\theta) = \sum_{j=1}^{T} [(U_{Bx}(\vec{x},t) - U_{Mx}(\vec{x},t;\theta))^2 + (U_{By}(\vec{x},t) - U_{My}(\vec{x},t;\theta))^2] \tag{4}$$

Eq. (4) represents the difference between the predicted trajectory and the buoy path. U_{Bx} and U_{By}, are the buoy velocity components in the x (W–E) and y (N–S) direction respectively; U_{Mx} and U_{My} are the model velocity components in the x and y direction respectively; T is the time period with buoy data and $\theta = (C_H, C_D, C_C)$ is the vector of parameters to be obtained.

Previous tests were performed including D in the calibration process as a parameter of θ. However, the best results were obtained without this coefficient. This is due to the fact that the random behaviour of the diffusive velocity is included in the confidence intervals of the advective model parameters (C_H, C_D and C_C).

The buoy velocity, $\vec{U}_B$, was obtained from the satellite tracked positions, which have a temporal resolution of 1 hour. The advective model velocity, $\vec{U}_M$, was calculated using Eq. (2) by means of the numerical data provided by the atmospheric models (wind and waves) and the radar currents collected during the experiment. The temporal resolution of the model velocity corresponds to a 3 hour time step.

The SCEM-UA algorithm provides N combinations of model parameters $\{\theta_i = (C_{Hi}, C_{Di}, C_{Ci}), i = 1...N\}$ that minimize the function $J(\theta)$. For each model parameter, the N values obtained in the calibration process were used to calculate the corresponding histogram and the cumulative distribution function. Based on this statistical information, the mean values $\hat{\theta} = (\hat{C}_H, \hat{C}_D, \hat{C}_C)$, and the confidence interval at a 95% confidence level were estimated.

2.3.3. Forcings set-up

In order to explore the relative importance of the three forcings and to decide which ones should be used for the experiment, the SCEM-UA algorithm was applied in a first step to obtain the optimal mean value and the 95% confidence interval of all three mentioned parameters (C_H, C_D and C_C) and to analyze the level of significance of each of them within the transport model. This result was used to configure the final experiment, as explained below.

In this analysis, the optimal coefficients were found to be $\hat{C}_H = -0.060$ included in the interval $(-0.125, 0.018)$, $\hat{C}_D = 0.025$ included in the interval (0.022,0.029) and $\hat{C}_C = 0.743$ in the interval (0.537,0.896). As can be observed, the wave coefficient $\hat{C}_H$ has a wide confidence interval ranging from negative to positive values. A confidence interval that includes the zero value indicates that this parameter is not statistically significant. Moreover, the negative mean value of $\hat{C}_H = -0.060$ does not represent a physical meaning. These results show that $\hat{C}_H$, in this particular case, is not a significant parameter, and in consequence could be discarded in the transport model. However, $\hat{C}_D$ and $\hat{C}_C$ show a narrow and positive confidence interval, implying that these parameters have statistical significance in the model.

Taking into account these results, in this study, the wave-induced Stokes drift was not considered to calculate the advective velocity (Eq. (2)). Therefore, the transport model was forced by numerical wind data and HF radar currents to compute the buoy trajectory.

3. Results

3.1. Calibration results

Once a final set-up of the experiment was designed, discarding the wave forcing, the transport model calibration was performed to obtain the optimal $\hat{C}_D$ for alternative 1 and the optimal $(\hat{C}_D, \hat{C}_C)$ combination for alternative 2.

The cumulative distribution function and the histogram of the model parameters obtained in alternative 1 and 2 are presented in Fig. 5. The 0.025 and 0.975 quantiles of the distribution function that define the upper and lower confidence interval limits are also shown.

With a 95% confidence level, the wind drag coefficient minimizing Eq. (4) was found to be $\hat{C}_D = 0.032$ included in the interval (0.029,0.035) for alternative 1 and $\hat{C}_D = 0.024$ included in the interval (0.020,0.027) for alternative 2. Both mean values are in the range reported in the literature (Reed et al., 1994; ASCE, 1996). The value $\hat{C}_D = 0.032$, calculated using only wind numerical

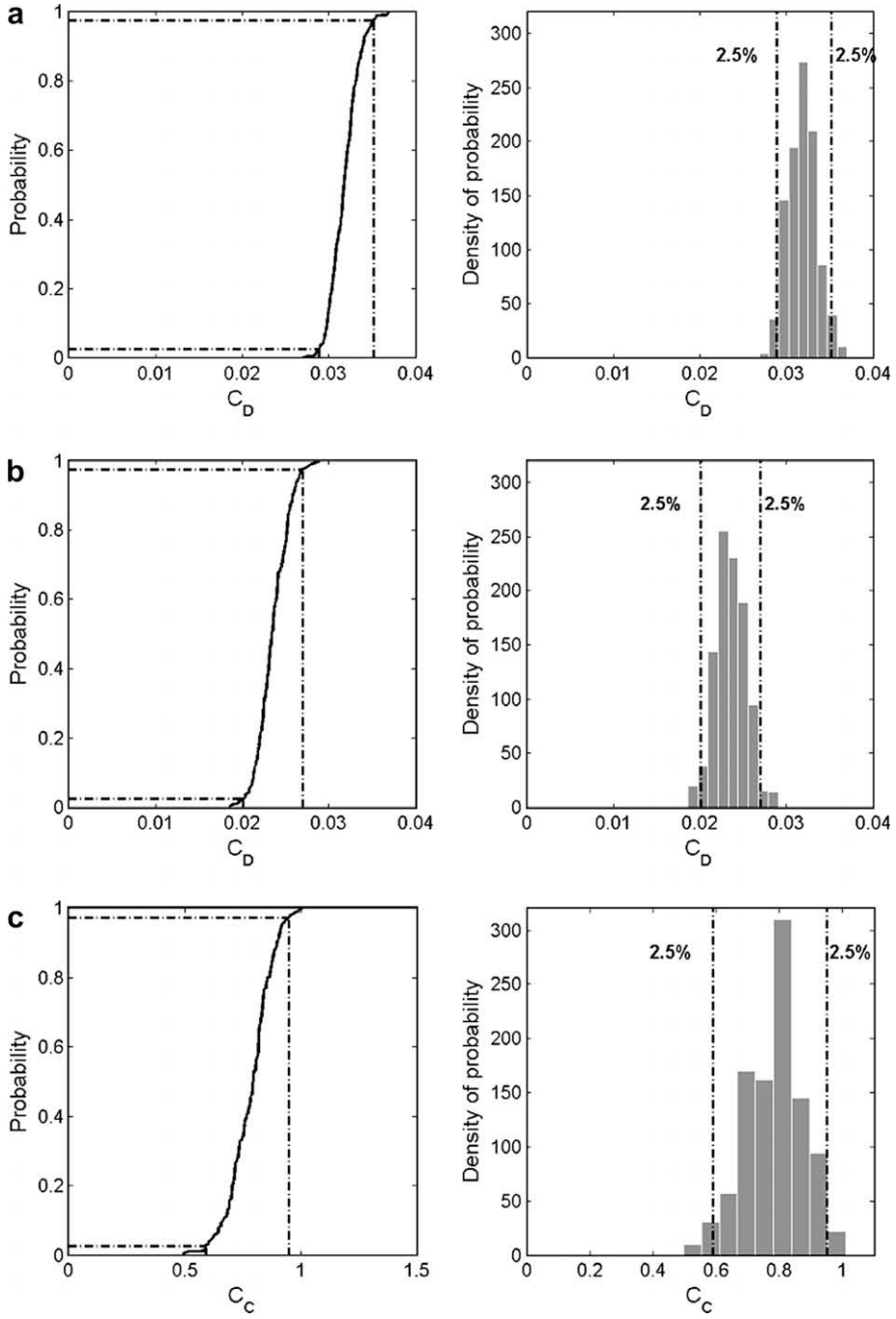

Fig. 5. Cumulative distribution function (left) and histogram (right) obtained in the calibration process. (a) C_D obtained in alternative 1. (b) C_D obtained in alternative 2. (c) C_C obtained in alternative 2. The 0.025 and 0.975 quantiles and the 95% confidence interval limits are represented by the dashed line.

data, corresponds to the most common value (3% of the wind speed) used in oil spill modeling. However, taking into account the currents (alternative 2), the wind forcing coefficient drops back to 0.024. This suggests that $\widehat{C}_D$, obtained in alternative 1, accounts for the wind-driven component resulting from the direct wind stress (sailing effect) and also from the wind-induced currents. However, in alternative 2, the wind and current effect are properly separated. In this case, the $\widehat{C}_D$ value accounts for wind drag forcing, whereas the HF radar currents contain the wind-induced component of the ocean surface current.

In alternative 2, the optimal current coefficient was found to be $\widehat{C}_C = 0.787$ included in the interval (0.591,0.949). Since C_C represents the effect of the current in a trajectory of a floating drifter, a value close to 1, like the one obtained with the radar, is desired. In contrast, using currents from global circulation models, Abascal et al. (2009) found a value of $\widehat{C}_C = 0.266$, suggesting discrepancies between the real and numerical current fields. Sotillo et al. (2008), using currents from higher resolution nested regional circulation models, obtained $\widehat{C}_C = 0.52$. These results show that the C_C value is improved using current data provided by regional circulation models. However, discrepancies between the real and numerical current fields are still present. The high C_C value obtained in the present study (close to 1) indicates a good agreement between the real current field and the radar HF current measurements, and shows the improvement of using observed HF currents radar instead of numerical model data.

3.2. Comparison of simulated and measured buoy velocity

The correlation factor between the model and buoy velocity components was calculated for each test. Scatter plot and the associated correlation factors for u (R_x^2) and v (R_y^2) components obtained in the first alternative are presented in Fig. 6. It is observed that the correlation is smaller than 0.7 for both components. To make a vectorial comparison between the model and the buoy velocity, the vector correlation factor, R^2, was calculated (Breaker et al., 2003). For a two-dimensional case R^2 varies between 0.0 (no correlation) and 2.0 (perfect correlation). In this case, the vectorial correlation, R^2, showed a value of 1.35.

Fig. 7 shows the results obtained in the second alternative. Comparing these results with those obtained in the first alternative (Fig. 6), an increase of the correlation factors is detected. The correlation factor changes from 0.67 to 0.71 in the x direction and from 0.68 to 0.74 in the y direction. This produces an improvement of the vectorial correlation factor, R^2, whose value changes from 1.35 to 1.45.

3.3. Trajectory analysis

The previously described TESEO transport model was used to reproduce the trajectory of the buoy during the study period. Two periods of the total buoy trajectory were selected based on the radar coverage area and the available current data (see Fig. 4). Thus, the analysis was performed for the positions of the buoy inside the radar domain. Each drifter period was divided into 24 h intervals, considering a total of 13 daily segments for the trajectory analysis. Simulations were carried out starting at the initial point of the intervals and using a 24 h forecast horizon, a typical prediction period in an emergency oil spill response.

For each proposed alternative, the daily segments were simulated using a Monte Carlo approach based on the calibration results. The SCEM-UA algorithm provided N ($N = 1000$) optimal set of parameters calculated by means of a Markov Chain Monte Carlo process. To include this information in the trajectory analysis, a high number of simulations (N) were performed considering the N set of optimal model parameters $\{(C_{Di},C_{Ci}) \ldots (C_{DN},C_{CN})\}$. The final position of the N simulated trajectories was different as a function of the combination of parameters used in the transport model see Eq. (2), providing an ensemble of numerical positions that defines the search area of the buoy location.

Each simulated trajectory was calculated as the mass centre of a cloud of 1000 independent numerical particles. Simulations were performed using a 60 sec time step. Because of the lack of information regarding the turbulence and the appropriate diffusion coefficients in the study area, this coefficient was considered to be 50 m^2/s, a value included in the interval reported in the literature (ASCE, 1996).

Fig. 8 shows the daily comparison between the buoy track and the simulated trajectories using numerical wind and measured HF

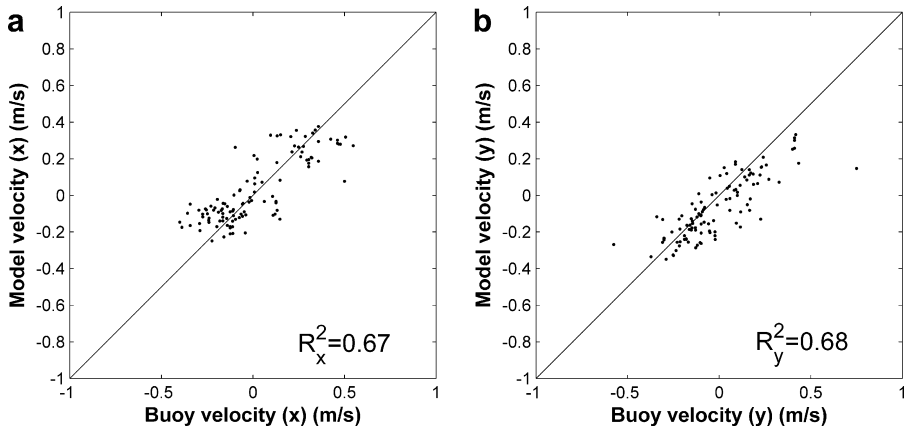

Fig. 6. Scatter plots of the model velocities versus buoy velocities for alternative 1. Correlation factors for the velocity component in the x direction (W–E) (R_x^2) and in the y direction (N–S) (R_y^2) are shown in panel a) and b).

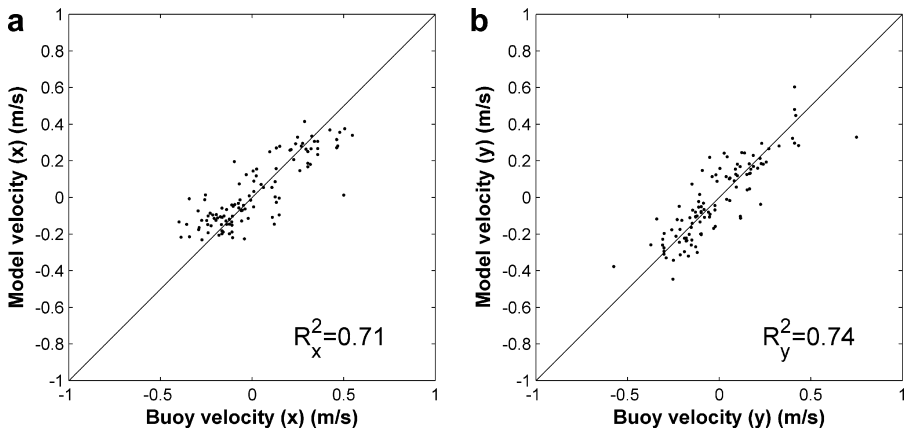

Fig. 7. Scatter plots of the model velocities versus buoy velocities for alternative 2. Correlation factors for the velocity component in the x direction (W–E) (R_x^2) and in the y direction (N–S) (R_y^2) are shown in panel a) and b).

radar currents (alternative 2). All simulations performed have not been presented in the figure for the purpose of clarity. The simulations not plotted have a similar degree of accuracy than the ones displayed in the figure. Simulations during the 1st period (from 12/22/2005 06:00 to 12/26/2005 00:00) and 2nd period (from 12/29/2005 06:00 to 01/08/2006 00:00) are displayed in Fig. 8a and b, respectively. In each panel of Fig. 8, the black line shows the actual buoy trajectory and the gray lines are the 1000 simulated trajectories for each daily period. The black dots show the numerical positions at the end of the 24 h simulation. As can be observed, a good agreement between the actual and the simulated trajectories was found.

The accuracy of the simulations was measured by the distance (d) between the actual and the simulated trajectories, defined as the minimum distance between the buoy position and the curve that contains 95% of the N simulated positions (95% confidence area). This distance was computed for every hour of each 24 h trajectory segment.

To evaluate the curve that delimits the 95% confidence area, a bivariate kernel estimator (Martinez and Martinez, 2002) was applied to calculate the two-dimensional density distribution for the N simulated positions. For a sample of size n, where each obser-

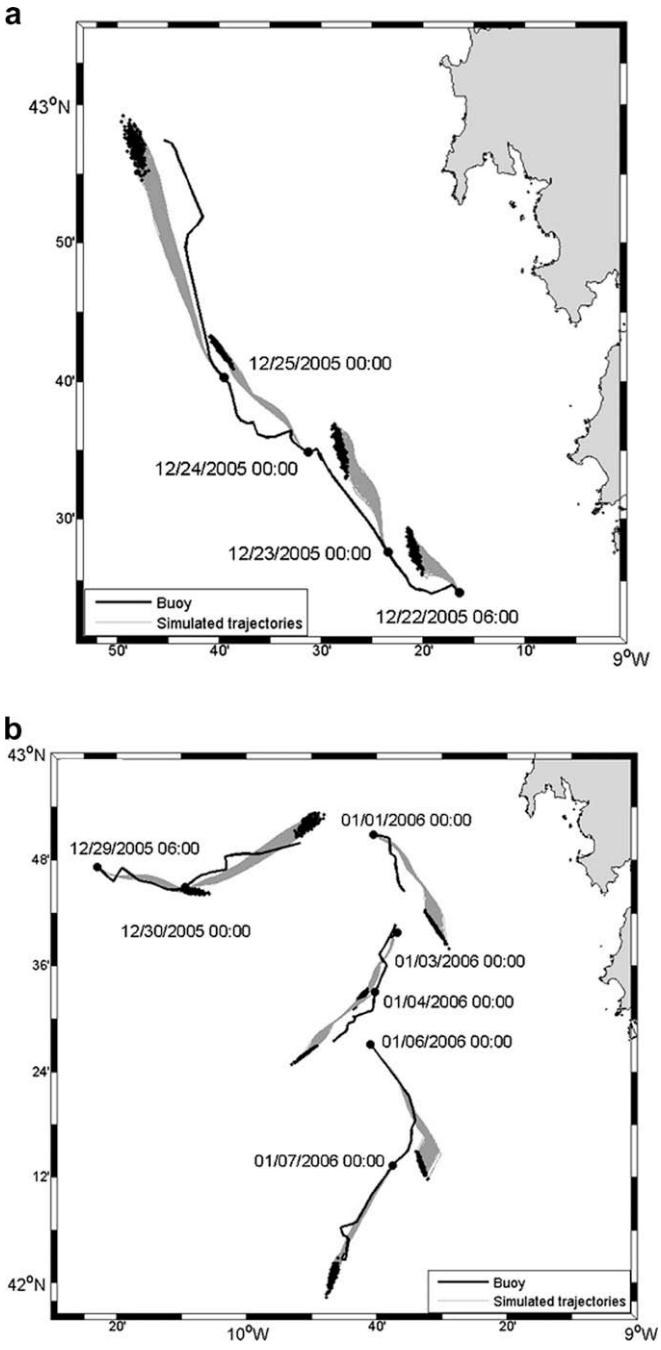

Fig. 8. Observed and simulated daily trajectories computed using wind and HF radar currents. Panel a) and b) correspond to the periods in which the buoy stayed inside the coverage area of the radar. The initial time and position of the simulations are indicated by the date and the black circles. The black dots stand for the final position of the 24 hour forecast period.

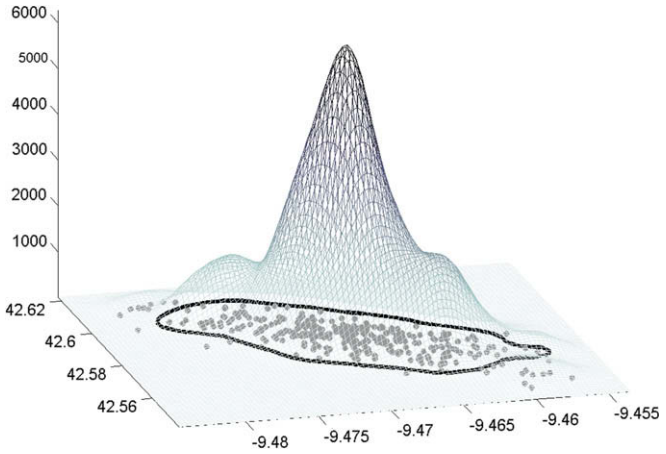

Fig. 9. Kernel density estimates for the final position of the simulated period 12/23/2005–12/24/2005. The black dots stands for the numerical positions of the 1000 simulated trajectories. The curve that includes 95% of the numerical data is represented by the black line.

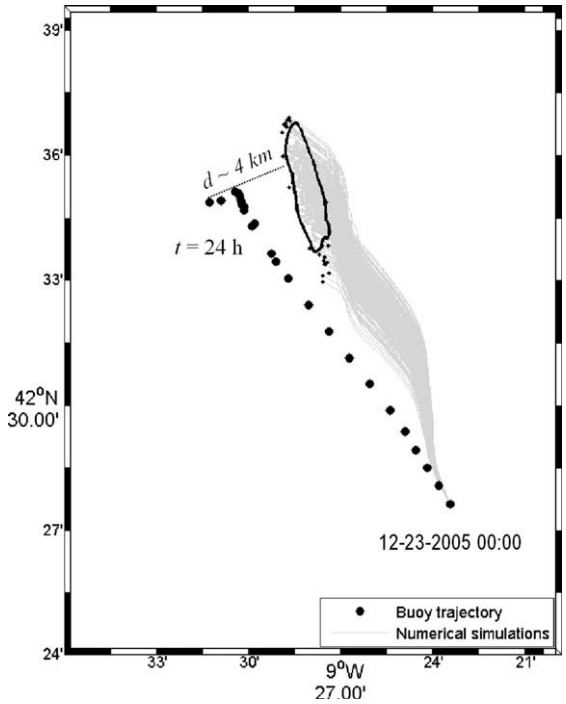

Fig. 10. Comparison between the buoy path and the simulated trajectories for the period 12/23/2005–12/24/2005. The curve that includes 95% of the final numerical positions is represented by the black line. The final separation (d) between the buoy location and the numerical results is about 4 km.

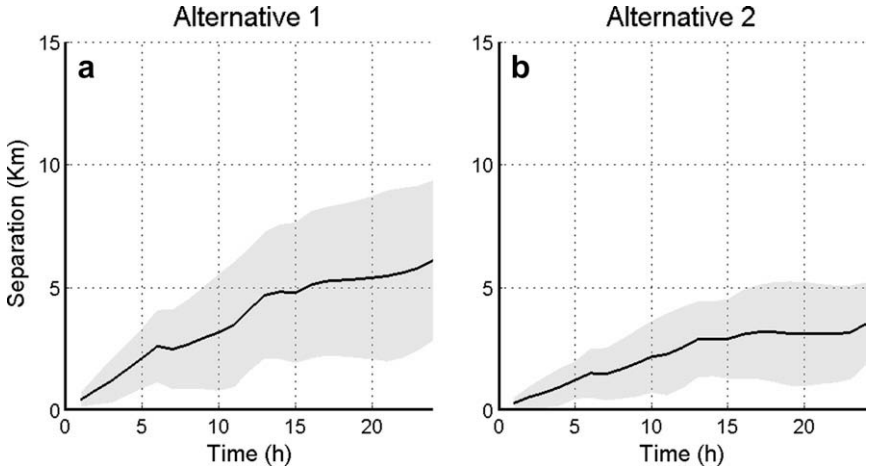

Fig. 11. Distance between the actual and simulated trajectories as a function of time (averaged over all simulated intervals). Panel (a) shows the difference for trajectories computed using wind numerical data and panel (b) the difference for trajectories calculated using wind and HF radar currents data. The mean value and the standard deviation are represented by the black line and the gray area, respectively.

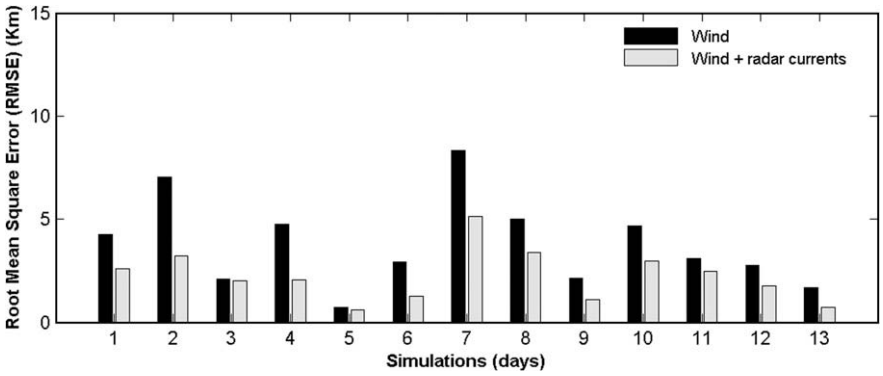

Fig. 12. *RMSE* for every daily simulation.

vation is a d-dimensional vector, X_i, $i = 1, \ldots, n$, the kernel density estimate is defined as (Martinez and Martinez, 2002):

$$\widehat{f}_{\mathrm{Ker}}(X) = \frac{1}{nh_1 \ldots h_{\mathrm{d}}} \sum_{i=1}^{n} \left\{ \prod_{j=1}^{d} K\left(\frac{x_j - X_{ij}}{h_j} \right) \right\} \tag{5}$$

where X_{ij} is the jth component of the ith observation, K is the kernel function and h is the smoothing parameter or window width. The parameter h is defined as

$$h_{j_{\mathrm{Ker}}} = \left(\frac{4}{n(d+2)} \right)^{\frac{1}{d+4}} \sigma_j; j = 1, \ldots, d, \tag{6}$$

where σ_j is the standard deviation of the jth component.The kernel equation for density estimation was considered as a Gaussian function:

$$K(x) = \frac{1}{\sqrt{2\pi}} \exp\left(\frac{-x^2}{2} \right) \tag{7}$$

As an illustrative example, Fig. 9 shows the kernel distribution function that corresponds to the final position of the simulated period 12/23/2005–12/24/2005 (see Fig. 8a). The black dots indicate the final position of the N simulated trajectories. The black line denotes the curve which includes 95% of the simulated data. The comparison between the buoy trajectory and the numerical simulations for the selected period is shown in Fig. 10. The curve that includes the 95% of the numerical positions at the end of the simulation (t = 24 h) is indicated by the black line. The positions outside of this curve are indicated by black dots. As can be observed in this figure, at the end of the 24 h period, d is about 4 km.

The distance (d) calculated for every hour of each 24 h simulation was averaged over all the daily simulations performed, according to the following equation

$$d_m(t) = \frac{1}{N} \sum_{i=1}^{N} \sqrt{d_i^2} \tag{8}$$

where d_m is the average hourly separation distance, t is the time and N is the number of 24 h periods simulated (N = 13).

Fig. 11 shows the mean temporal evolution (black line) and standard deviation (grey area) of the hourly difference between the actual and modelled trajectory for alternative 1 (panel a) and 2 (panel b). In both cases, the distance between actual and simulated buoy positions increases over time. However, it is important to note that the mean separation is always smaller when HF radar currents are used to compute the motion of the buoy. After 24 h, the distance between the real and simulated position is $\sim$6 ± 3.3 km in alternative 1 and $\sim$3.5 ± 1.7 km in alternative 2. The error for each daily simulated period was estimated by means of the root mean squared error, RMSE

$$\mathrm{RMSE} = \sqrt{\frac{1}{T} \sum_{i=0}^{T} d_i^2} \tag{9}$$

where T is the 24 h period.

Fig. 12 shows a comparison between the RMSE calculated in both alternatives. The results indicate that the positions obtained when integrating HF surface currents show lower errors. The maximum RMSE for all simulations is 8.3 km for alternative 1. Using HF radar currents for the simulation of the trajectories, these values decrease to 5.1 km. The minimum RMSE is less than 1 km for both alternatives, giving a satisfactory result.

The daily variation in RMSE could be explained by temporal inaccuracies in the current or wind field. The higher RMSE daily simulations could be improved by adjusting the model parameters to the specific periods. However, the results of performing the individual analysis for shorter daily periods with temporal inaccuracies of forcing data could contribute to the generation of coefficients without a physical meaning, being the results useless for a real future situation.

It is important to note that, for practical reasons, the squared difference between the simulation and actual buoy position is a better error index than the simple linear distance. This is due to the fact that the search and rescue operations are based within the area of exploration and, therefore only the surface to be scanned before finding the drifting object has been taken into account. Therefore, the search area was calculated in terms of circles of maximum RMSE radium, obtaining 219 km^2 and 83 km^2 for alternative 1 and 2, respectively. These results show that by considering HF radar currents to simulate the buoy motion, the mean search and rescue area is reduced, on average, by approximately 62%.

4. Conclusions

In this paper, the contribution of the HF radar technology for oil spill modelling and trajectory analysis of floating objects was studied using a Lagrangian trajectory model. A methodology to optimize the transport model performance and to determine the search area of the predicted positions was developed and applied to data collected during the Galicia HF Radar Experience.

The transport model was calibrated using the SCEM-UA algorithm in order to obtain the optimal value of the parameters and to analyze their level of significance in the transport model. The analysis showed that in this particular case, the wave coefficient (C_H) was not a significant parameter of the model, and therefore the wave-induced Stokes drift could be discarded in the transport model.

To evaluate the benefits of the HF radar currents, the buoy trajectory was simulated using only wind numerical data (alternative 1) and wind numerical data and observed HF radar currents (alternative 2). For each alternative, the model was calibrated and the mean value and the 95% confidence interval were obtained. Results of the calibration show that the optimal mean $\widehat{C}_D$ value decreases from $\widehat{C}_D$ = 0.032 (alternative 1) to $\widehat{C}_D$ = 0.024 when HF radar currents are included in the analysis. This means that wind and current effects are properly separated, indicating that $\widehat{C}_D$ = 0.024 accounts for wind drag forcing whereas the HF radar currents contain the wind-induced component of the ocean surface current. The high $\widehat{C}_C$ value obtained suggests a quite good agreement between the real current field and the radar HF current measurements. The correlation factors obtained in both experiments showed a good agreement between the buoy trajectory and the numerical velocities. For the first alternative, R_x^2 =0.67 and R_y^2 =0.68 were estimated. Although these values correlated well with the buoy trajectory, the correlation is improved $R_x^2 = 0.71$ and $R_y^2 = 0.74$ considering HF radar currents. These results represent an improvement with respect to similar analysis performed using numerical currents data (Abascal et al., 2009).

The buoy trajectory was computed by means of a Monte Carlo simulation using the N optimal combination of model parameters obtained in the calibration process. Comparisons of actual and simulated trajectories showed the value of HF radar currents for the estimated buoy motion. In general, the analysis integrating HF radar currents were more accurate than those performed considering only wind numerical data. The time evolution of the mean hourly distance between the simulated and the real drifter positions shows that the separation is always smaller when including HF radar currents (see Fig. 11). After 24 h of simulated trajectories, a distance of ~6 ± 3.3 km (alternative 1) and ~3.5 ± 1.7 km (alternative 2) was found. This result is also supported by the RMSE calculated for every daily simulation, which shows that the lowest errors are obtained using HF radar currents. The maximum RMSE for the first alternative is 8.3 km, which is reduced to 5.1 km for the second alternative. Taken into account that the search and rescue operations are based within the area of exploration, the effect of introducing HF radar in practical operations is highlighted. The simulation performed with HF radar currents reduces the search and rescue area on average by approximately 62% compared to the simulation not containing this data. These differences in the search and rescue area can be critical when, for example, a person is in the water and there is a risk of hypothermia.

This study has demonstrated that measured data provided by the HF radar, combined with atmospheric forecast models, are of value for trajectory analysis of floating objects.

Although the validation has been performed using a drifter buoy, the results could be also applied for other floating objects or floating substances like oil slicks. However, further study is required to analyze the differences between the buoy and oil spill transport and the reasons for the different degree of accuracy of the simulations from one day to another. Moreover, future work is required considering several buoys in the analysis. The spatial variability and the turbulence diffusion of the region could be studied based on the drift of a set of buoys released at the same place and time. Using this information in the proposed methodology could improve the estimation of the search area.

Acknowledgments

This work has been partly funded by the Spanish Ministry of Education and Science under the research project TRA2007-65133/TMAR (PREVER project). The authors would like to thank the Agencia Estatal de Meteorología, Qualitas–REMOS, AA.PP Vigo and Coruña for the collaboration and the data provided for the study. The second author would like to thank the Spanish Ministry of Science and Technology for the support under Ramon y Cajal Program.

References

Abascal, A.J., Castanedo, S., Gutierrez, A.D., Comerma, E., Medina, R., Losada, I.J., 2007. TESEO, an operational system for simulating oil spills trajectories and fate processes. Proceedings, ISOPE-2007: the 17th International Offshore Ocean and Polar Engineering Conference Lisbon, Portugal. The International Society of Offshore Ocean and Polar Engineers (ISOPE) 3, 1751–1758.

Abascal, A.J., Castanedo, S., Mendez, F.J., Medina, R., Losada, I.J., 2009. Calibration of a Lagrangian transport model using drifting buoys deployed during the *Prestige* oil spill. Journal of Coastal Research. doi:10.2112/07–0849.1.

Alfonso, M., Álvarez, E., López, J.D., 2006. Comparison of CODAR SeaSonde HF Radar operational waves and currents measurements with Puertos del Estado buoys. Final report. Puertos del Estado, 32.

Alvarez-Fanjul, E., Alfonso, M., Ruiz, M.I., López, J.D., Rodríguez, I., 2003. Real time monitoring of Spanish coastal waters: the deep water network 2002. In: Dahlin, H. et al. (Eds.), Building the European Capacity in Operational Oceanography: proceedings of the 3rd International Conference on EuroGOOS 3–6. Elsevier Oceanography Series, Athens Greece 69, pp. 98–402.

Alvarez-Fanjul, E., Losada, I., Tintoré, J., Menéndez, J., Espino, M., Parrilla, G., Martinez, I., Muñuzuri, V.P., 2007. The ESEOO Project: developments and perspectives for operational oceanography at Spain. Proceedings, ISOPE-2007:

the 17th International Offshore Ocean and Polar Engineering Conference. Lisbon, Portugal. The International Society of Offshore Ocean and Polar Engineers (ISOPE) 3, 1708–1715.
ASCE, 1996. State-of-the-art review of modeling transport and fate of oil spills, ASCE committee on modeling oil spills water resources engineering division. Journal of Hydraulic Engineering 122 (11), 594–609.
Breaker, L.C., Gemmill, W.H., deWitt, P.W., Crosby, D.S., 2003. A curious relationship between the winds and currents at the western entrance of the Santa Barbara Channel. Journal of Geophysics Research 108 (C5), 3132, 1-1–3132, 1-21.
Caballero, A., Espino, M., Sagarminaga, Y., Ferrer, L., Uriarte, A., González, M., 2008. Simulating the migration of drifters deployed in the Bay of Biscay, during the Prestige crisis. Marine Pollution Bulletin 56 (3), 475–482.
Carretero, J.C., Álvarez, E., Gómez, M., Pérez, B., Rodriguez, I., 2000. Ocean forecasting in narrow shelf seas: application to the Spanish coasts. Coastal Engineering 4, 269–293.
Castanedo, S., Medina, R., Losada, I.J., Vidal, C., Méndez, F.J., Osorio, A., Juanes, J.A., Puente, A., 2006. The Prestige oil spill in Cantabria (Bay of Biscay) Part I: operational forecasting system for quick response, risk assessment and protection of natural resources. Journal of Coastal Research 22 (6), 1474–1489.
Cats, G., Wolters, L., 1996. The Hirlam project. IEEE Computational Science and Engineering 3 (4), 4–7.
Chapman, R.D., Shay, L.K., Graber, H.C., Edson, J.B., Karachintsev, A., Trump, C.L., Ross, D.B., 1997. On the accuracy of HF radar surface current measurements: intercomparisons with ship-based sensors. Journal of Geophysics Research 102 (8), 18737–18748.
Chapman, R.D., Graber, H.C., 1997. Validation of HF radar measurements. Oceanography 10, 76–79.
Dean, R.G., Dalrymple, R.A., 1991. Water wave mechanics for engineers and scientists. Advanced Series on Ocean Engineering 2. World Scientific, Singapore.
Duan, Q., Sorooshian, S., Gupta, V., 1992. Effective and efficient global optimization for conceptual rainfall-runoff models. Water Resources Research 28 (4), 1015–1031.
Edwards, K.P., Werner, F.E., Blanton, B.O., 2006. Comparison of observed and modeled drifter trajectories in coastal regions: an improvement through adjustments for observed drifter slip and errors in wind fields. Journal of Atmospheric and Oceanic Technology 23 (11), 1614–1620.
González, M., Uriarte, A., Pozo, R., Collins, M., 2006. The Prestige crisis: operational oceanography applied to oil recovery, by the Basque fishing fleet. Marine Pollution Bulletin 53, 369–374.
Hodgins, D.O., 1991. New capabilities in real-time oil spill and fate prediction using HF radar remote sensing. Proceedings The 14th AMOP Technical Seminar, Canada.
Hunter, J.R., Craig, P.D., Phillips, H.E., 1993. On the use of random walk models with spatially variable diffusivity. Journal Comparative Physiology 106, 366–376.
Kohut, J.T., Roarty, H.J., Glenn, S.M., 2006. Characterizing observed environmental variability with HF Doppler Radar surface current mappers and acoustic Doppler Current profilers: environmental variability in the Coastal Ocean. Journal of Oceanic Engineering 31 (4), 876–884.
Komen, G.J., Cavaleri, L., Donelan, M., Hasselmann, K., Janssen, P.A.E.M., 1994. Dynamics and Modeling of Ocean Waves. Cambridge University Press, UK.
Maier-Reimer, E., 1982. On tracer methods in computational hydrodynamics. In: Abbott, M.B., Cunge, J.A. (Eds.), Engineering Application of Computational Hydraulics, 1. Pitman, London. Chapter 9.
Martinez, W.L., Martinez, A.R., 2002. Computational Statistics Handbook. Boca Raton Florida, Chapman and HallCRC (Chapter 8).
Ministerio de Medio Ambiente, 2005. Dirección General de Costas, La catástrofe del Prestige. Limpieza y restauración del litoral norte peninsular, pp. 288 (in Spanish).
Montero, P., Blanco, J., Cabanas, J.M., Maneiro, J., Pazos, Y., Moroño, A., Balseiro, C.F., Carracedo, P., Gomez, B., Penabad, E., Pérez-Muñuzuri, V., Braunschweig, F., Fernandes, R., Leitao, P.C., Neves, R., 2003. Oil spill monitoring and forecasting on the Prestige-Nassau accident Proc. Environment Canada's 26th Artic and Marine Oil spill (AMOP) Technical Seminar. Otawa, Canada, 1013–1029.
Nittis, K., Zervakis, V., Perivoliotis, L., Papadopoulos, A., Chronis, G., 2001. Operational monitoring and forecasting in the Aegean Sea: system limitations and forecasting skill evaluation. Marine Pollution Bulletin, 43 (7–12), 154–163.
O'Donnell, J., Ullman, D., Spaulding, M., Howlett, E., Fake, T., Hall, P., Tatsu, I., Edwards, C., Anderson, E., McClay, T., Kohut, J., Allen, A., Lester, S., Lewandowski, M., 2005. Integration of Coastal Ocean Dynamics Application Radar (CODAR) and Short-Term Prediction System (STPS) surface current estimates into the search and rescue Optimal Planning System (SAROPS), US. Coast Guard Tech. Rep., DTCG39-00-D-R00008/HSCG32-04-J-100052.
Pinardi, N., Allen, I., Demirov, E., De Mey, P., Korres, G., Lascaratos, A., Le Traon, P.-Y., Maillard, C., Manzella, G., Tziavos, C., 2003. The Mediterranean ocean forecasting system: first phase of implementation (1998–2001). Annales Geophysicae, 21, 3–20.
Price, J.M., Reed, M., Howard, M.K., Johnson, W.R., Ji, Z., Marshall, C.F., Guinasso JR, N.L., Rainey, G.B., 2006. Preliminary assessment of an oil-spill trajectory model using a satellite-tracked, oil-spill-simulating drifter. Environmental Modelling and software 21, 258–270.
Reed, M., Turner, C., Odulo, A., 1994. The role of wind and emulsification in modelling oil spill and surface drifter trajectories. Spill Science and Technology Bulletin 1 (2), 143–157.
Sebastiao, P., Soares, C.G., 2006. Uncertainty in predictions of oil spill trajectories in a coastal zone. Journal of Marine Systems 63, 257–269.
Sotillo, M.G., Alvarez Fanjul, E., Castanedo, S., Abascal, A.J., Menendez, J., Olivella, R., García-Ladona, E., Ruiz-Villareal, M., Conde, J., Gómez, M., Conde, P., Gutierrez, A.D., Medina, R., 2008. Towards an operational system for oil spill forecast in the Spanish waters: initial developments and implementation test. Marine Pollution Bulletin 56 (4), 686–703.
Ullman, D., O'Donnell, J., Edwards, C., Fake, T., Morschauser, D., Sprague, M., Allen, A., Krenzien, B., 2003. Use of coastal ocean dynamics application radar (CODAR) technology in US coast guard search and rescue planning US. Coast Guard Rep. CG-D-09-03, 40.
Ullman, D.S., O'Donnell, J., Kohut, J., Fake, T., Allen, A. 2006. Trajectory prediction using HF radar surface currents: Monte Carlo simulations of prediction uncertainties. Journal of Geophysics Research, 111, C12005, 1–14.
Vrugt, J.A., Gupta, H.V., Bouten, W., Sorooshian, S., 2003. A shuffled complex evolution metropolis algorithm for optimization and uncertainty assessment of hydrologic model parameters. Water Resources Research, 39 (8), 1201(1–8), 1–16.
Vrugt, J.A., Gupta, H.V., Bouten, W., Sorooshian, S., 2003. Shuffled complex evolution metropolis (SCEM-UA) algorithm. Manual Version 1.0, 24.
WAMDI Group, Hasselman, S.K., Janssen, P.A.E.M., Komen, G.J., Bertotti, L., Lionello, P., Guillaume, A., Cardone, V.C., Greenwood, J.A., Reistad, M., Zambresky, L., Ewing, J.A., 1988. The WAM model - A third generation ocean wave prediction model. Journal of Physical Oceanography 18, 1775–1810.